Revista de la Academia Colombiana de Ciencias Exactas, Físicas y Naturales.
46(180):628-645, julio-septiembre de 2022. doi: https://doi.org/10.18257/raccefyn.1723

Ciencias Físicas

Artículo original

Rare-earth ferrobismuthites: ferromagnetic ceramic semiconductors with applicability in spintronic devices

Ferrobismutitas de tierra rara: cerámicos ferromagnéticos semiconductores con aplicabilidad en dispositivos espintrónicos

Jairo Roa-Rojas[1,*], Javier A. Cuervo Farfán[1], Críspulo E. Deluque Toro[2], David A. Landínez Téllez[1,3], Carlos A. Parra Vargas[4]

[1] Grupo de Física de Nuevos Materiales, Departamento de Física, Universidad Nacional de Colombia, Bogotá, D.C., Colombia
[2] Grupo de Nuevos Materiales, Facultad de Ingeniería, Universidad del Magdalena, Santa Marta, Colombia
[3] Grupo de Estudios de Materiales GEMA, Departamento de Física, Universidad Nacional de Colombia, Bogotá, D.C., Colombia
[4] Grupo de Física de Materiales, Escuela de Física, Universidad Pedagógica y Tecnológica de Colombia, Tunja, Colombia

Inaugural article for admission of Jairo Roa-Rojas, as a full member of the Colombian Academy of Exact, Physical and Natural Sciences

Abstract

We report here the synthesis process of the perovskite-like complex material $Bi_{0.5}R_{0.5}FeO_3$ (R=Eu, Sm, Dy) using the ceramic method, as well as its structural, optical, magnetic, and electrical characterizations. Refined X-ray diffraction data revealed that this material crystallizes in an orthorhombic structure (space group Pnma number 62). The band gap value in the optical response shown in the diffuse reflectance spectroscopy curve was typical of semiconductor materials. The magnetization exhibited a very low coercive field hysteretic behavior, which is characteristic of weak ferromagnetism, for all temperatures examined below 300 K and the various magnetic fields applied. The real and complex electric permittivity curves showed the occurrence of dielectric relaxation processes at 113 K in agreement with reports of pyroelectric and thermo-stimulated currents as a function of temperature revealing the appearance of ferroelectric polarization below 113 K with possible magnetoelectric coupling. On the other hand, we made a theoretical study of the electronic structure with and without the inclusion of a Berry distortional phase and ab-initio calculations following the density functional theory formalism and the pseudopotential plane wave method. In this formalism, the exchange and correlation mechanisms are described by the generalized gradient approach (GGA + U) considering spin polarization. The Berry phase analysis suggested the occurrence of ferroelectricity at temperatures below 113 K consistent with the experimental analysis evidencing a biferroic behavior at low temperatures given that the distortional phase introduces hybridizations between the 3d-Fe and 2p-O states favoring the appearance of Dzyaloshinskii-Moriya interactions, which, in turn, facilitate the appearance of ferroelectricity coexisting with a weak ferromagnetism. The thermodynamic properties in the presence or absence of the Berry phase by means of the Debye quasi-harmonic model revealed the appearance of a ferroelectric transition at 113 K, which corroborates their magnetoelectric nature at low temperatures. The ferromagnetic semiconducting character found at room temperature enhances this material for applications in spintronics technology.

Keywords: Perovskite; Structure; Ferromagnetism; Ferroelectricity; Semiconductor; Spintronics.

Resumen

Se reporta el proceso de síntesis del material complejo de tipo perovskita $Bi_{0.5}R_{0.5}FeO_3$ (R=Eu, Sm, Dy) mediante el método cerámico, así como su caracterización estructural, óptica, magnética y eléctrica. Los datos refinados de difracción de rayos X revelaron que este material cristaliza en

Citation: Roa-Rojas J, Cuervo Farfán JA, Deluque Toro CE, *et al*. Rare-earth ferrobismuthites: ferromagnetic ceramic semiconductors with applicability in spintronic devices. Revista de la Academia Colombiana de Ciencias Exactas, Físicas y Naturales. 46(180):628-645, julio-septiembre de 2022. doi: https://doi.org/10.18257/raccefyn.1723

Editor: Diógenes Campos Romero

***Corresponding autor:**
Jairo Roa Rojas; jroar@unal.edu.co

Received: June 30, 2022
Accepted: August 9, 2022
Published on line: September 9, 2022

una estructura ortorrómbica (grupo espacial Pnma número 62). La respuesta óptica en la curva de espectroscopia de reflectancia difusa proporcionó un valor de brecha energética típico de los materiales semiconductores. La magnetización presentó un comportamiento histerético de campo coercitivo muy bajo, característico del ferromagnetismo débil, para todas las temperaturas examinadas por debajo de 300 K y la aplicación de varios campos magnéticos. Las curvas de permitividad eléctrica real y compleja evidenciaron la presencia de procesos de relajación dieléctrica a 113 K, lo que concuerda con los reportes sobre corrientes piroeléctricas y termoestimuladas en función de la temperatura y revela la aparición de polarización ferroeléctrica por debajo de los 113 K, con un posible acoplamiento magnetoeléctrico. Por otro lado, se hizo un estudio teórico de la estructura electrónica con y sin la fase distorsiva de Berry. Se hicieron cálculos ab *initio* siguiendo el formalismo de la teoría funcional de la densidad y el método de ondas planas pseudopotenciales, formalismo en el cual los mecanismos de intercambio y correlación se describen mediante el enfoque de gradiente generalizado (GGA + U) considerando la polarización de espín. El análisis con la fase de Berry sugirió la presencia de ferroelectricidad a menos de 113 K, lo que concuerda con el análisis experimental que sugiere un comportamiento biferroico a bajas temperaturas debido a que la fase distorsiva introduce hibridaciones entre los estados 3d-Fe y 2p-O que favorecen la aparición de interacciones Dzyaloshinskii-Moriya, las cuales, a su vez, facilitan la aparición de ferroelectricidad en condiciones de ferromagnetismo débil. Las propiedades termodinámicas en presencia y ausencia de la fase de Berry en el modelo cuasi-armónico de Debye revelaron la aparición de una transición ferroeléctrica a los 113 K, lo que corrobora la naturaleza magnetoeléctrica a bajas temperaturas. El carácter ferromagnético semiconductor a temperatura ambiente potencia este material para aplicaciones en tecnología espintrónica.

Palabras clave: Perovskita; Estructura; Ferromagnetismo; Ferroelectricidad; Semiconductor; Espintrónica.

Introduction

Since the 19th century, the development of physical laws related to the phenomena of electric charge transport was the basis for significant advances in communications, industry, transportation, power generation, and the design of technology for personal and home use, among others. All the technological innovations of the 20th century have been associated with the movement of electric charges determining the concept of electric current. On the other hand, Maxwell's electrodynamics establishes that such movement of charge is intrinsically related to a magnetic response. Oersted, Faraday, Ampère, and Lenz, among others, determined the intensities and directions of the fields produced by the occurrence of electric currents. These fields turned out to be analogous to those evidenced in magnets, in which the forces of attraction or repulsion on some metallic objects have their origin in the movement of electric charges within the atoms, the interactions of these charges with neighboring atoms, and the presence of external magnetic fields. Specifically, the orbital motion of the electron, which is nothing but charge in motion, can be conceived as a current in a loop that creates a very small magnetic field (orbital magnetic moment). Similarly, the rotation of the electron around its own axis in one direction or another is still charge in motion, giving rise to the so-called spin magnetic moment.

According to the Pauli exclusion principle, the atom full electron shells contain electrons distributed in orbitals within which only two can be located: one with spin up and the other with spin down, which explains why the contributions of atoms full shells to the magnetic response of the material are negligible and respond to interactions of the atoms with their neighbors, and why the valence electrons are mostly responsible for the magnetic "tendencies" of some elements. Thus, in the presence of an external magnetic field, a material can exhibit a negative response that opposes the applied field due to the application of Lenz's law at the molecular level. This behavior, observed in more than 30 elements of the periodic table at room temperature, was called *diamagnetism* by Faraday, who perceived that in these materials the direction of the induced currents must oppose the direction of the cause that produces them.

Revista de la Academia Colombiana de Ciencias Exactas, Físicas y Naturales.
46(180):628-645, julio-septiembre de 2022. doi: https://doi.org/10.18257/raccefyn.1723

At room temperature, a second group of about 50 elements in the periodic table responds positively as long as they are subjected to an external magnetic field. In these so-called paramagnetic materials, the percentage of the response effect (magnetization) is much greater than the diamagnetism mentioned above as a result of one of the well-known Hund's rules according to which an arrangement of electrons with the same spin orientation in the different possible orbitals of the valence electrons is energetically more favorable than the pairing of the same electrons. The higher the number of unpaired electrons, the higher the effective magnetic moment in the unit cell of the material, the highest values being those observed in some rare earths such as Dy, Ho, Tb, and Er, whose number of f orbitals facilitates the possibility of finding up to seven unpaired electron spins.

On the other hand, the most relevant magnetic responses for technological applications are ferromagnetism, antiferromagnetism, and ferrimagnetism. In these three types of response, the materials behave as paramagnetic at high temperatures while below a transition temperature, the ordering of the magnetic moments changes due to the presence of interaction potentials between them. In the former, these interactions give rise to magnetic domains and Bloch walls that decrease the internal energy of the materials, so that below the Curie temperature, where the material is ferromagnetic, the application of positive and negative external fields makes it possible to observe one of its main characteristics: the hysteresis curve. This curve shows three parameters that depend on the specific composition of each material: the so-called coercive field, the saturation magnetization, and the remanent magnetization. The type of technological application depends on their values: for example, high values of these three parameters suggest the design of permanent magnets while low coercive field and high saturation and remanent magnetizations are ideal in devices designed to read and record information on magnetic media. At room temperature, three elements of the periodic table exhibit a ferromagnetic response: Fe, Co, and Ni. In the second group, below the so-called Néel temperature, the interactions between magnetic moments in the domains facilitate the minimum energy for oppositely oriented spins. Finally, in ferrimagnetic materials, a type of incomplete antiferromagnetism occurs determining a majority of spins oriented in the direction and sense of the applied field, so that the material shows a hysteresis curve very similar to that of ferromagnetic materials.

In the cases of ferro-, antiferro- and ferrimagnetic materials, the presence of cations with valence electrons in the 3d, 4d, and 4f orbitals can lead to the occurrence of the so-called crystalline field which, in turn, promotes their splitting in high and low spin orbitals (**Estrada-Contreras *et al.,*** 2021). This behavior is energetically compensated by structural distortions characterized by the Jahn-Teller effect. As if this were not enough, the type of chemical bonding between the nearest neighbour atoms can be of the bonding, anti-bonding, or non-bonding type where the accumulation of electric charge in the electronic orbitals can adopt various arrangements favoring some interactions and harming others. These phenomena introduce modifications in the exchange mechanisms between valence electrons of neighboring atoms giving rise to exotic magnetic responses, such as giant and colossal magnetoresistance, half-metallicity, multiferroicity, and magnetic semiconductivity, which have unsuspected uses in the emerging spintronics industry.

Classical electrodynamics allows defining the current density of electric charge transport as a function of carrier number density, the value of the electron charge, and its velocity. However, it is well-known that in metallic materials the carriers are the valence electrons and that in semiconductors these electrons are not free and require excitation to bridge the band gap and reach the so-called conduction band. We must not forget, however, the spin of electrons participating in the electric transport, which in metals and semiconductors is symmetrical in the sense that an equal number of electrons with spin up and spin down carry the electric charge. If it is not symmetrical, as is the case in half-metallic materials, where the material is conductive for one of the spin orientations and insulating for the other, or in ferromagnetic semiconductors, where the band gap is smaller for one of the spin orientations than for the other, one could speak of spin transport in addition to charge transport. Thus, a definition of spin current arises which, in analogy with

traditional electrodynamics, should depend on the number of carriers, the transport rate, and the spin value (½) and not on the charge value of the electric case ($1.6x10^{-19}$ c). The control of the variables that determine the spin currents is the object of spintronics. Such control can be affected by the generation of spin states, the application of external fields, the introduction of spin-orbit type mechanisms, the application of electromagnetic waves, the inclusion of elements generating orbital splitting, the inclusion of thermal gradients, the application of mechanical rotations, and even by geometrical modifications in the material.

In the present report, we present the perovskite-type ceramic material $Bi_{0.5}R_{0.5}FeO_3$ (R=Eu, Sm, Dy) that evidences measurable physical responses associated with processes promising future application in spintronics. We will explain in detail the family to which the material under study belongs, the synthesis process, the crystallographic analysis, the electrical behavior, the optical response, and the magnetic character of the perovskite-type material $Bi_{0.5}R_{0.5}FeO_3$ (R=Eu, Sm, Dy), as well as the implications and perspectives in the design of technological devices classified as belonging to the spintronics industry.

Perovskite-type materials

A family of versatile materials that represents a large percentage of the systems currently investigated in solid physics and chemistry is constituted by the so-called perovskites. In general, perovskites correspond to the ideal formula ABX_3, where A is an alkaline earth element, a rare earth, or a metal or semimetal of large ionic radius, B represents a transition metal or a lanthanide element, and X is usually oxygen or a halogen (**Hazen,** 1988). Modifications of the atomic radii of A and B introduce structural distortions and new crystalline phases while inclusions of rare earth elements enable the production of materials with exotic electrical and magnetic properties (**Llamosa *et al.,*** 2009). Partial substitutions of the A cation give rise to complex $A_{0.5}A'_{0.5}BO_3$ materials (**Triana *et al.*,** 2012; **Cuervo-Farfán *et al.,*** 2017). Their chemical configuration offers multiple possibilities for combining different elements, as well as the feasibility of synthesizing new materials with a wide variety of physical properties. Depending on the magnetic and electrical characteristics of A, A', and B it is relatively easy to create new perovskite-type systems with promising prospects in the new field of spintronic technology (**Cuervo-Farfán *et al*.,** 2016). In this family of perovskite materials, the A and A' cations adopt an arrangement in the form of horizontally intercalated sheets or columnar plane-like layers (**King & Woodward,** 2010). These structural features constrain the crystal symmetries for the different families of complex perovskites suggesting the occurrence of structural distortions that also correspond to octahedral tilts and rotations that influence the physical properties as a result of the intrinsic characteristics of the material constituents (**Benedek,** 2014).

The results regarding the structural properties and the electrical, magnetic, and optical responses of materials belonging to these families of perovskite-type materials were correlated with the predictions from the density of electronic states and band structure calculations. We made the calculations using the density-functional theory (DFT), which has become a potentially powerful tool for predicting the physical properties of perovskite-type materials (**Landínez-Téllez *et al.,*** 2014). Moreover, considering that the macroscopic thermodynamic properties are strongly correlated with the microscopic dynamics of the atoms of the material, and assuming that the collective vibrations of the crystal lattices in these solid materials take place through phonons, it is possible to study the fundamental excitations associated with these thermodynamic properties. The most representative function of phonons occurs in insulators and semiconductors, where they make direct contributions to properties such as the specific heat and thermal expansion indicating that they are temperature-dependent properties. As for phonons, we considered vibrations in perovskite-type crystals as having a harmonic character valid for temperature values below the Debye temperature of the solid. In this sense, theoretical methods can constitute a complementary tool for the study of atomic dynamics at relatively high temperatures by means of approximations such as the quasi-harmonic Debye model (**Deluque-Toro *et al.,*** 2018). In the present work, we present the results of

the density of electronic states and the behavior of specific heat, the Debye temperature, the entropy, the thermal expansion, and the Grüneisen parameter as functions of pressure and temperature.

The single perovskite-type material $RFeO_3$, known as rare-earth orthoferrite, has been widely investigated for more than 60 years for its G-type antiferromagnetic character (**Koehler & Wollan,** 1957), as well as for exhibiting simultaneously weak ferromagnetic (**Phokha *et al*.,** 2014) and ferroelectric (**Acharya *et al*.,** 2010) responses, for which it can be classified as a multiferroic material (**Spaldin,** 2020). Experimentally, it has been observed that the rare-earth orthoferrite $RFeO_3$ adopts an orthorhombic crystal structure belonging to the Pnmb space group (number 62), with a tolerance factor of τ=0.951 and octahedral distortions given by $a^+b^-b^-$ (**Dann *et al.,*** 1994). On the other hand, the bismuth-based perovskite $BiFeO_3$ has also been widely studied because it exhibits very interesting physical properties with great technological potential. In particular, it shows multiferroicity at temperatures close to room temperature (**Lu *et al*.,** 2010). This material has a rhombohedral structure (space group R3c) at T=300 K (**Xu *et al*.,** 2009) evidencing antiferromagnetism below the Néel temperature (T_N) of ≈640 K and ferroelectricity at temperatures below the Curie temperature (T_C) of ≈1100 K (**Wu *et al,*** 2010). When the bismuth ferrite $BiFeO_3$ binds to the rare-earth orthoferrite $RFeO_3$ described above, it allows the formation of a complex structure of the $Bi_{0.5}R_{0.5}FeO_3$ type (**Cuervo-Farfán *et al.,*** 2018; **Nieto-Camacho *et al.,*** 2020; **Garrido *et al.,*** 2021).

Experimental procedures

The $Bi_{0.5}R_{0.5}FeO_3$ (R=Eu, Sm, Dy) samples were synthesized using the conventional solid-state method, i.e., by reacting the high purity precursor oxides produced by Aldrich (99.99% purity): R_2O_3 (R=Eu, Sm, Dy), Bi_2O_3, and Fe_2O_3. After weighing them in stoichiometric proportions, the powders were inhomogeneously mixed for 3 h in an agate mortar, and then the mixture obtained was subjected to the thermal process of calcination at 550°C for 36 h. The material was homogenized in an agate mortar for 30 min and then crushed in an acetone binder environment under an axial pressure of 500 MPa for 15 min to obtain disk-shaped samples. Finally, sintering intermediate grinding processes were carried out at 600°C, 715°C, and 810°C for 24 h each. Structural analysis of the samples was performed using a PANalytical X'pert-Pro X-ray diffractometer ($\lambda Cu_{K\alpha}$=1.540598 Å) in the Bragg-Brentano configuration with a 0.001° step at 2θ and 10 s time. The structural analysis was performed by Rietveld-type refinement to determine the crystallographic properties of the material. The complex impedance was measured as a function of temperature using an Agilent-4194A phase gain and impedance analyzer, a Janis Research cryogenic system (model VPF-475), and a Lake Shore 332 temperature controller. These measurements were done at a temperature variation rate of 1.7 K/min and a frequency range between 102 and 107 Hz. The I-V curve at room temperature was produced from data measured on a Keithley-6517A DC electrometer and a sample holder with gold-plated silver contacts designed and adapted to the cryogenic system and temperature controller by the authors. The band gap and energy excitation regimes at room temperature were examined using a VARIAN Cary 5000 UV-Vis-NIR diffuse reflectance spectrophotometer (DRS) provided with an integrating sphere with a PMT/Pbs detector. The magnetic response was evaluated by measuring magnetization as a function of temperature using the zero field cooling (ZFC) and field cooling (FC) procedures under different magnetic field strengths. Likewise, magnetic hysteresis was measured by varying the applied field strength in isothermal curves at different temperatures. To measure the magnetic response, we used a VSM-PPMS Quantum Design. Several temperatures and applied field regimes were considered for the different samples measured.

Theoretical calculations

To study of structural, cohesive, electronic, and thermodynamic properties of complex perovskites, we used the VASP code based on the density-functional theory (DFT) and the projector of augmented waves (PAW) (**Perdew *et al.,*** 1996; **Heyd *et al.,*** 2003). Since the

generalized gradient approximation (GGA) does not fully describe the system containing 3d-Fe, 3d-Co, and 5d-R orbitals, the exchange and correlation energy was evaluated using the GGA with the corrections to the Hubbard U-potential (GGA+U) (**Estrada Contreras *et al*.,** 2021; **Guss *et al*.,** 2014). Due to the ferromagnetic characteristic of the material, the U value was obtained by the method described for this type of magnetic ordering (**Liechtenstein *et al.*,** 1995) finding optimal potentials UFe=#.# eV. Ion-electron interactions were described through PAW (**Blöchl,** 1994; **Kresse & Joubert,** 1999) and all calculations were performed considering spin-polarized configurations. The kinetic energy cutoff for the plane wave expansion of the electronic wave function was 520 eV. We used k-points gratings defined according to the Monkhorst-Pack method (**Monkhorst & Pack,** 1976) verifying their convergence until obtaining an energy accuracy over 1 meV/atom. We used the Methfessel-Paxton technique (**Methfessel & Paxton,** 1986) to fill the electronic levels with a mixing factor of 0.1 eV. For these configurations, we considered gratings of 9x9x7 k-points, which represent 284 k-points in the irreducible Brillouin zone. We used the conjugate gradient method to find stable ionic positions with an energy value of 0.1 meV as the convergence criterion for the total self-consistent energy calculations. The lattice parameters and internal coordinates of the unit cell were fully optimized by maintaining the spatial symmetry group of the crystal structure until the forces were less than 30 meV/Å and the energy due to ionic relaxation below 1.0 meV/atom. These calculations were performed considering an orthorhombic structure with space group Pnma (number 62) (**Jaramillo-Palacio *et al.,*** 2017; **Jaramillo-Palacio *et al.,*** 2021; **Gil-Rebaza *et al.,*** 2021; **Cuervo-Farfán *et al*.,** 2020). To determine the density of states (DOS) parameters, we calculated the total energy (E) and external pressure (P) for different volumes (V) varying from the equilibrium volume (V0) up to ± 5% and allowing relaxation of the internal coordinates. The bulk modulus (B0) and its pressure derivative (B') were obtained by fitting the pressure curves as a function of volume from the Murnaghan equation of state (**Murnaghan,** 1944).

The thermodynamic calculations were done following the Debye quasi-harmonic model (**Deluque-Toro *et al*.,** 2018a; **Deluque-Toro *et al.,*** 2018b) where macroscopically measurable thermophysical properties are directly associated with the atoms microscopic dynamics within the material when subjected to pressure and temperature external changes. Considering that the collective vibrations of the crystalline cells of solids occur in the form of phonons, the fundamental excitations associated with these thermodynamic properties can be conveniently calculated. In materials with relatively high electrical resistivities, phonons play a particularly important role in providing relevant contributions to some properties such as the specific heat and the thermal expansion as functions of the temperature. Thus, it is expected that the vibrations of the crystal lattice exhibit a harmonic character for temperature values below the Debye temperature of the material. In this work, we applied the Debye quasi-harmonic model as part of the study of atomic dynamics in the appropriate temperature regime.

Crystal structure

Once the samples were obtained, we proceeded to the structural characterization by obtaining an X-ray diffraction pattern (XRD) at room temperature followed by a careful Rietveld analysis of the experimental data. The results of this analysis revealed that the most stable crystallization structure corresponded to the Pnma space group (number 62) characteristic of orthorhombic perovskite-type materials (**Cuervo-Farfán *et al*.,** 2020; **Cuervo-Farfán *et al.*,** 2018; **Nieto-Camacho *et al*.,** 2020). For this crystalline system, an octahedral tilt of the type $a^+b^-b^-$, characterized by the existence of two rotation angles with similar magnitude values and opposite directions, is expected. This distortion is not commensurable with the displacement of Fe cations (**Glazer,** 1975), so this material is not expected to show ferroelectric properties at room temperature.

The structural exemplification in **figure 1**a shows the typical octahedral distortions of the material where A represents 50% Bi and 50% rare earth, and B=Fe. The out-of-phase inclinations of the FeO_6 octahedra produced along the b and c axes are also shown.

Revista de la Academia Colombiana de Ciencias Exactas, Físicas y Naturales.
46(180):628-645, julio-septiembre de 2022. doi: https://doi.org/10.18257/raccefyn.1723

Due to Glazer's octahedral tinting, the …O-Fe-O-Fe-O… bonds extend in a zigzag path along the *b* and *c* axes of the crystal cell. These distortions are best observed in **figures 1b** and **1c**, where they are seen to cause differences in the O-Fe-O bond distances along the three octahedral sub-axes, as well as in the Fe-O-Fe bond angles between octahedra. The interatomic distances between Fe^{3+} cations and O^{2-} anions are denoted as a_1, a_2, and a_3, with 1.99 Å ≤ a_i ≤ 2.06 Å and $a_1 \neq a_2 \neq a_3$. On the other hand, the bond angles in the three crystallographic directions are denoted as φ_1 and φ_2, such that $\varphi_1 > \varphi_2$ and $146^o < \varphi_i < 152^o$. The partial cause of these distortions has to do with the differences in the ionic radius between the R^{3+} (1.08 Å ≤ R^{3+} ≤ 1.24 Å) and Bi^{3+} (1.03 Å) cations in the cuboctahedral coordination occupying the same crystallographic sites as shown in **figure 1a**. Additionally, the electrostatic interactions between the outermost electron orbitals of these ions subtly modify the interatomic distances a_i and bond angles φ_i affecting the electrical and magnetic responses of the material. Besides the differences between the O-Fe-O distances in the three sub-axes of the octahedra, there are several factors allowing for the evaluation of the degree of distortion of the crystallographic cell. One of them is the so-called tolerance factor (**Goldschmidt**, 1926), which considers a ratio between the ionic radii of cations and anions according to the expression $\tau=[½(r_A+r_{A'})+r_O]/\sqrt{2}(r_B+r_O)$ where $r_A=r_{Bi}$ and $r_{A'}=r_R$ are the ionic radii of Bi^{3+} and R^{3+} in cuboctahedral coordination, $r_B=r_{Fe}$, the ionic radius of Fe^{3+} in octahedral coordination, and r_O, the ionic radius of O^{2-}. The further away from the ideal value τ=1 expected for a cubic cell without octahedral inclinations, the greater the structural distortion of the material. For the materials analyzed, τ_{Eu}= 0.9111, τ_{Sm}=0.9136, and τ_{Dy}=0.8983; it can be inferred, then, that the greatest distortion occurs for R=Dy while the least asymmetric cell takes place for R=Sm.

Another measure of the distorting effects may be predicted by the global instability index (GII), which is given by the root mean square deviation of the experimental bond valence sums from the atomic valence (**Brown,** 2009) $GII = \sqrt{\frac{\sum_{i=1}^{N}(d_i)^2}{N}}$, where N is the number of ions and d is the bond discrepancy factor defined as the deviation of the bond valence sum from the formal valence (**Yamada *et al.***, 2018). The values obtained are GII_{Eu}= 0.03890, GII_{Sm}=0.01719, and GII_{Dy}=0.16771. For perovskite-type materials the expected *GII* values < 0.2 have the highest probability of synthesis (**Lufaso & Woodward,** 2001), so it is inferred that the most stable structure corresponds to R=Sm and the least stable R=Dy (although synthesizable by having *GII*<2).

The optimal distortional magnitude relative to the octahedral tilt and size of octahedra in the crystallographic cell can be estimated by means of the bond valence model, which allows the quantitative description of the inorganic bonding in ionic solids (**Lufaso & Woodward,** 2001). The bond valence s_{ij} associated with each cation-anion interaction is calculated using $s_{ij}=exp[(R_{ij}-d_{ij})/B]$, where d_{ij} is the cation-anion distance. The parameter B

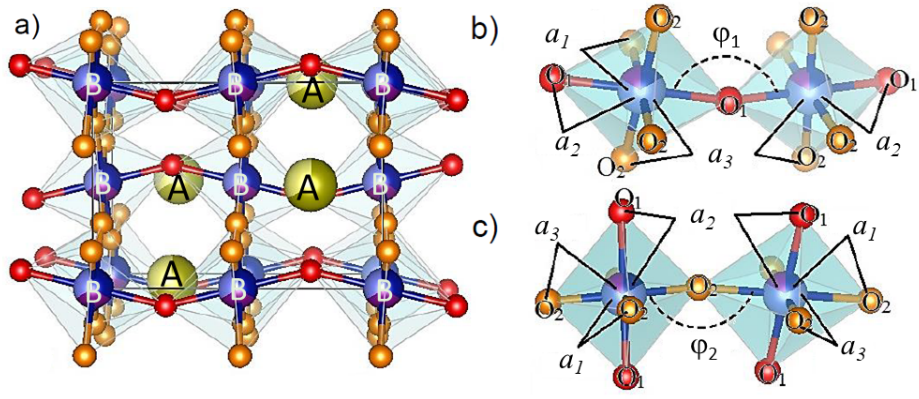

Figure 1. Exemplification of structural properties for $Bi_{0.5}R_{0.5}FeO_3$ perovskites where the A sites are occupied by Bi^{3+} and R^{3+} cations while the B sites correspond to Fe^{3+}

is determined empirically but it can often be treated as a universal constant with a value of 0.37. R_{ij} is found empirically for each cation-anion pair based on a large number of well-determined bond distances for the cation-anion pair under analysis. The bond valence sum (BVS) V_i of the A, B, and X ions is calculated by summing the individual bond valences (s_{ij}) on each ion according to the equation $V_i=\sum s_{ij}$. In the calculations, it is important to take into account the coordination number 6 for Fe^{3+} cations and 12 for R^{3+} and Bi^{3+}, as well as the variations in bond distances due to Glazer distortions. The values found for BVS suggest that the degree of structural distortion in this family of materials increases with the increasing ionic radius of the R^{3+} cation.

Optical characteristics

To experimentally establish the optical response of the material, diffuse reflectance spectroscopy measurements were performed in the 200 nm < λ < 1400 nm wavelength regime as shown in **figure 2a**. Three regimes denoted by wavelengths λ_1, λ_2, and λ_3 are clearly observed in the figure for the three materials under study. These regimes have place for the energy regions 3.3 eV ≤ E_1 ≤ 3.6 eV, 1.9 eV ≤ E_2 ≤ 2.2 eV, and 1.0 ≤ E_3 ≤ 1.3 eV.

The excitations of the three energy regimes mentioned above coincide with the irreducible representation for vibrations given by $\Gamma=5_{RSM}+7B1u+9B2u+9B3u$, where 5_{RSM} represents five vibrational modes observed through Raman spectroscopy while $7B1u+9B2u+9B3u$ corresponds to three modes observable by DRS in the three regions previously determined in the UV-Vis-NIR spectrum shown in **figure 2a** (**Cuervo-Farfán *et al.*,** 2021). These three energy regimes are related to vibrations in the octahedral Fe-O bonds and in the cuboctahedral R-O and Bi-O bonds (**Sorescu *et al.*,** 2011).

The analysis method to determine the band gap from this type of spectra is the usual one, which in some cases follows the classical Kubelka-Munk method (**Myrick *et al.*,** 2011) as shown in **figure 2b**. When dealing with a polycrystalline material with strongly granular morphology and subject to the existence of homogeneities, the band gap value E_g should be considered as a macroscopic average influenced by several factors: gap values

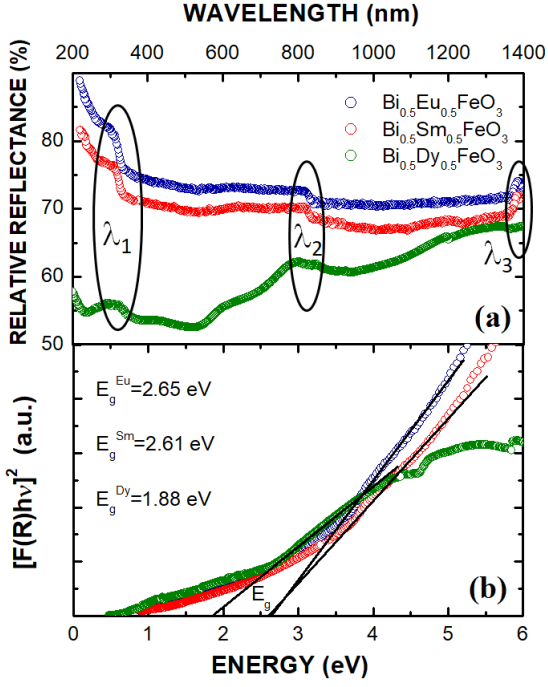

Figure 2. DRS spectrum **(a)** and Kubelka-Munk analysis **(b)** for the determination of the band gap in the $Bi_{0.5}R_{0.5}FeO_3$ compounds

Revista de la Academia Colombiana de Ciencias Exactas, Físicas y Naturales.
46(180):628-645, julio-septiembre de 2022. doi: https://doi.org/10.18257/raccefyn.1723

lower than E_g due to charge carriers at the grain boundaries perpendicular to the current direction; values higher than E_g due to insulating grain boundaries, and the potential caused by the porous character of the samples. Under these considerations, the average band gap obtained for the family of perovskites under study was $E_g^{Eu} = 2.65$ eV, $E_g^{Sm} = 2.61$ eV, and $E_g^{Dy} = 1.88$ eV.

Magnetic feature

To examine the magnetic character of the $Bi_{0.5}R_{0.5}FeO_3$ family of perovskite-type materials, isotherm curves at 50, 200, and 300 K temperatures of magnetization as a function of the applied field were carried out in the -30 kOe ≤ H ≤ 30 kOe for R=Eu, Sm and -50 kOe ≤ H ≤ 50 kOe regimes for R=Dy as shown in **figure 3**.

The figure shows the occurrence of a weak ferromagnetic response. The corresponding magnetic parameters in **table 1** show a tendency for the coercive field to grow with the increasing effective magnetic moment of the unit cell and decreasing ionic radius of the rare earth cation while the remnant magnetization decreases.

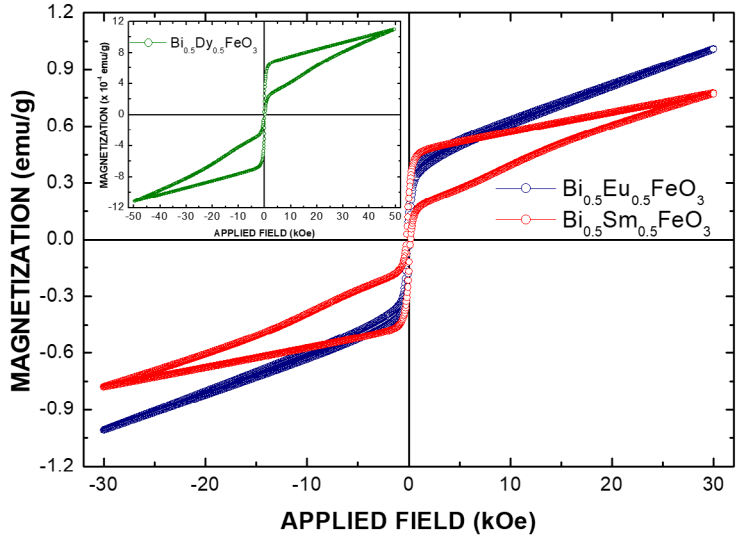

Figure 3. Weak ferromagnetic behavior measured at 300 K by magnetization curves as a function of applied field strength for $Bi_{0.5}R_{0.5}FeO_3$ material (R=Eu and Sm). The inset shows the magnetization for R=Dy, which evidences a difference of three orders of magnitude with respect to R=Eu and Sm.

Table 1. Magnetic parameters observed for the $Bi_{0.5}R_{0.5}FeO_3$ perovskite-like structures

Material	μ_{eff} (μ_B)	R ionic radius (Å)	T (K)	H_C (Oe)	M_R (emu/g)	REF
$Bi_{0.5}Sm_{0.5}FeO_3$	5.8	1.24	50	240	0.29	**Cuervo-Farfán *et al.***, 2020
			200	194	0.24	
			300	151	0.20	
$Bi_{0.5}Eu_{0.5}FeO_3$	5.9	1.12	50	296	0.14	**Cuervo-Farfán *et al***, 2018
			200	225	0.09	
			300	190	0.05	
$Bi_{0.5}Dy_{0.5}FeO_3$	9.5	1.08	50	700	$3.25x10^{-4}$	**Nieto-Camacho *et al***, 2020
			200	448	$2.63x10^{-4}$	
			300	300	$2.63x10^{-4}$	

In other words, ferromagnetism tends to soften as the magnetic moment of the unit cell increases and with the chemical compression of the cuboctahedral sub-cell where the cation R, whose ionic radius decreases, is located. This soft character of the ferromagnetic response could have technological utility in devices requiring a fast switching of magnetic spins, which can be achieved by applying low external fields H≤700 Oe.

Some features of interest such as the occurrence of narrow magnetic hysteresis and linear character without saturation at relatively high fields in the magnetization curves of **figure 3** are worth mentioning. The linear tendency above the hysteretic behavior in this type of polycrystalline volumetric material could respond to the presence of submicrometer-sized grains, some of them constituted by ferromagnetic monodomains that would give rise to a superparamagnetic type response (see references in **table 1**). The absence of saturation for the applied H field strengths prevents the determination of the effective magnetic moment of the unit cell and it should be noted that for this reason, the values for μ_{eff} in **table 1** are essentially theoretical.

Electric response

The complex impedance measurements as a function of temperature for the three materials of $Bi_{0.5}R_{0.5}FeO_3$ (R=Eu, Sm, and Dy) revealed the occurrence of a marked dispersion of the complex electric permittivity and evidenced Maxwell-Wagner-type relaxation processes that manifested in a substantial increase of the real part of the electrical permittivity (ε') with increasing temperature (**Cuervo-Farfán *et al.,*** 2020; **Cuervo-Farfán *et al.,*** 2018). These processes are considered electrically inhomogeneous due to incipient microscopic conduction mechanisms in the dielectric response (**Lunkenheimer *et al.,*** 2002).

On the other hand, in the low-temperature regime, the change in electrical permittivity starts very close to T=113 K. As reported for R=Sm (**Cuervo-Farfán *et al.,*** 2020), in this thermal region the real electrical permittivity varies logarithmically with applied frequency and temperature, which allows determining an Arrhenius-like behavior of the electrical conductivity ac as a function of temperature. The onset of this region, marked with an arrow in **figure 4b**, coincides with the measurements of pyroelectric currents and

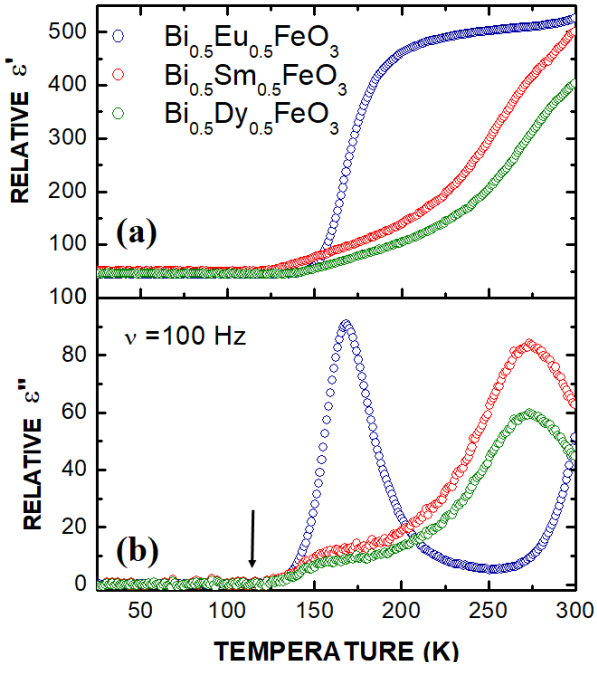

Figure 4. (a) Real and **(b)** complex electrical permittivity as a function of temperature measured on samples of $Bi_{0.5}R_{0.5}FeO_3$ material in a 100 Hz frequency

Revista de la Academia Colombiana de Ciencias Exactas, Físicas y Naturales.
46(180):628-645, julio-septiembre de 2022. doi: https://doi.org/10.18257/raccefyn.1723

thermo-stimulated currents for R=Eu (**Cuervo-Farfán *et al.*,** 2018) according to which this temperature value would coincide with the occurrence of a structural transition from a centrosymmetric to a non-centrosymmetric crystal lattice implying simultaneous effects of ferroelectric polarization with the ferromagnetic response, which would suggest that below T=113 K this family of materials would evidence multiferroic properties.

This behavior responds to the eventual superposition of space charge factors due to the accumulation of free electrons in the grains and intergranular boundaries reducing the resistivity at high temperatures; oxygen vacancies; accumulation of interfacial distortions, and the presence of different polarization mechanisms, among others. It can be assumed, then, that the processes involved in electronic transport correspond to the thermally-activated type and originated through mechanisms related to the ceramic properties of the material that contribute to the electrical conductivity of the composite, such as small polarons associated with lattice deformation, probably with free charges, ionization, or intrinsic ionic conductivity (**Dash *et al.*,** 2014).

The semiconductor behavior at room temperature was experimentally established through I-V curves, as shown in **figure 5**. The behavior observed in the I-V curves is clearly nonlinear, fitting an equation of the type $I=I_oV^z$ known as the figure of merit of varistor-type semiconductors, where I_o is a free constant and z represents the nonlinear coefficient, which generally has non-integer values between 1 and 2 (**Pandey *et al.*,** 2015). The values obtained for the nonlinear coefficient in the figure of merit of the varistor are in the $1.32<z<1.46$ regime and reveal the growth of the conductivity with the increasing applied field.

According to the nonlinear characteristic of the curves, the increase in the applied voltage promotes an increase in the electrical conductivity manifested in the growth of the slope of the curves suggesting that the applied electric field increases the number of free charge carriers participating in the electrical conduction as expected in semiconductor materials. In the meantime, the varistor-type character originates from the polycrystalline and granular character of the material following the figure of merit in the form of a potential function since its boundaries have micro-junctions acting as circuits formed by microscopic diodes whose conductivity increases with the increment of the applied field because the intra-granular transport current flow dominates over the resistance represented by the inter-granular junctions (**Vojta *et al.*,** 1996).

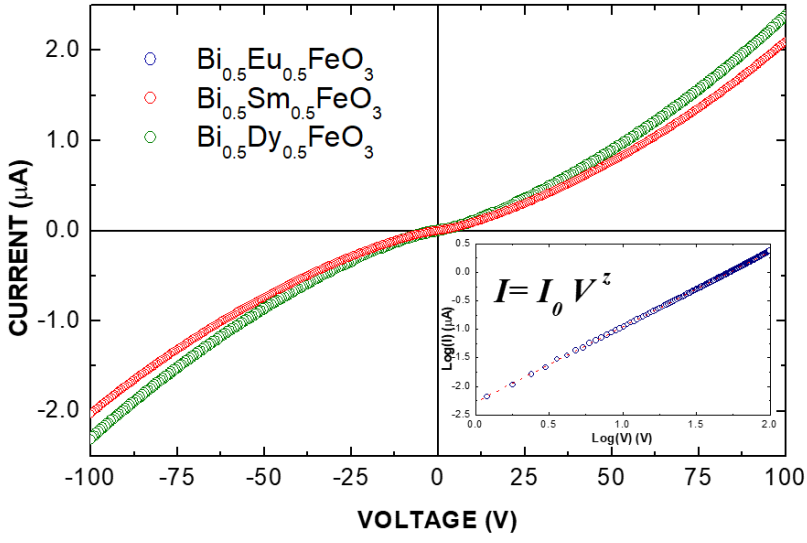

Figure 5. Measured I-V curves for materials with R=Sm and Dy. The inset shows the power-law behavior characteristic of the varistor-type semiconductor response for R=Eu.

Electronic properties and phase transition

DFT has proven to be a powerful tool in the prediction of various physical properties in perovskite-like materials (**Alarcón-Suesca *et al.,*** 2019). To establish the magnetic and semiconducting character of the $Bi_{0.5}R_{0.5}FeO_3$ materials under analysis, we calculated the total density of states considering the structural group Pnma (number 62) for R=Eu (**Cuervo-Farfán *et al.*,** 2018), R=Sm (**Cuervo-Farfán *et al.,*** 2020), and R=Dy (**Garrido *et al.*,** 2021). In all three cases, the total density of states exhibited the behavior exemplified in **figure 6a** for R=Dy considering the up and down spin orientations around the Fermi energy denoted as E_F for E=0 eV. Two relevant features are clearly observed in the figure: first, the difference between the densities of states for the two spin orientations is a finite value, which guarantees a value of the effective magnetic moment of the unit cell corresponding to that expected from the application of Hund's rules; second, the material exhibits an insulator character for the up-spin polarization ($E_g^{\uparrow}$=3.49 eV) and a semiconducting one for the other spin orientation ($E_g^{\downarrow}$=1.76 eV). **Figure 6b** schematizes the type of non-symmetric behavior of the band gap for the two spin configurations, one of the characteristics identifying ferromagnetic semiconductor materials (**Garrido *et al.*,** 2021) that were experimentally established in this manuscript.

The difference between the band gaps for the two (up and down) spin polarizations is very interesting from a technological point of view, particularly for the design of spintronic devices, as an energy excitation in the 1.76 eV<E<3.49 eV range enables the transport of electric charge in the material and, besides, makes it possible to generate a -½ spin current and the production of spin valves and polarized spin currents.

Given the experimental results suggesting the possibility of ferroelectric ordering at temperatures below 113 K, the Berry phase is used to calculate the density of electronic states in this family of materials (**Gil Rebaza *et al.*,** 2021). This methodology is applicable because spontaneous ferroelectric polarization is intrinsically related to structural phase transitions between centrosymmetric and non-centrosymmetric cells. Thus, electronic properties in the $Bi_{0.5}R_{0.5}FeO_3$ family of materials can be calculated by introducing octahedral distortions in the Pnma space group cell that characterizes the crystals of these materials.

These structural distortions have been accounted for previously by calculating the Berry's phase of the electronic Bloch wave functions at zero temperature and in the absence of an applied electric field, i.e., as a spontaneous polarization in a ferroelectric

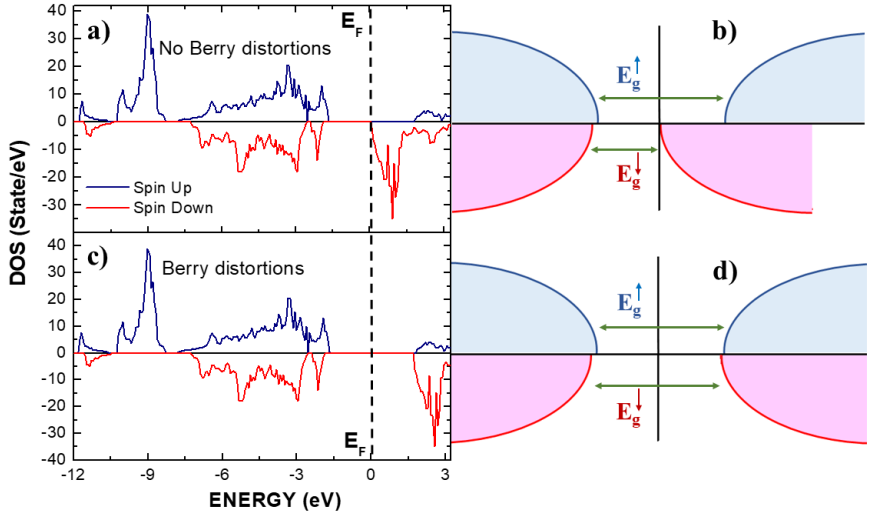

Figure 6. Total state density with and without the Berry phase (**a** and **c**, respectively), and band scheme of the ferromagnetic semiconductor **(b)** and biferroic semiconductor **(d)** for the $Bi_{0.5}Dy_{0.5}FeO_3$ complex perovskite

Revista de la Academia Colombiana de Ciencias Exactas, Físicas y Naturales.
46(180):628-645, julio-septiembre de 2022. doi: https://doi.org/10.18257/raccefyn.1723

material (**Resta,** 1994; **Resta,** 1997). This calculation is made in the absence of an external electric field, so the polarization process is understood as resulting from the dynamics of the network. Thus, a transition associated with microscopic displacements of the Fe cations from their structural sites of symmetry in the FeO_6 octahedra can be expected.

The results of the total density of states for the two spin-up and spin-down polarizations under the distortional effect for R=Dy are presented in **figure 6c**. The most notable characteristics are the tendency of the material to adopt an insulating nature for the two spin orientations eliminating the semiconductor character and the permanence of the ferromagnetic behavior in accordance with the experimental results for R=Eu, Sm, and Dy, respectively (**Cuervo-Farfán *et al*.,** 2018; **Cuervo-Farfán *et al*.,** 2020; **Nieto-Camacho *et al*.,** 2020). The average band gap calculated for the two spin orientations from the curves in **figure 6c** is 3.5 eV. A graphical representation of the band gap modification around the Fermi level can be seen in **figure 6d**, where the impossibility of obtaining polarized spin currents when the Berry transition takes place at low temperatures is clearly observed. Additionally, an electric polarization curve appears gradually when Berry's distortion is performed (**Gil Rebaza *et al*.,** 2021).

Finally, it is relevant to establish the possible occurrence of a phase transition between the ferromagnetic semiconductor state at high temperatures and the coexistence of ferromagnetism and ferroelectricity at low temperatures after Berry distortion. For this purpose, the specific heat curves as a function of temperature were obtained without distortion and with Berry's octahedral distortion for R=Eu (**figure 7**).

As shown in the inset of **figure 7**, the difference between the specific heat values (with and without the Berry phase) evidences an abrupt change for the value close to ΔC=113 K consistent with the experimental results reported for R=Eu (**Cuervo-Farfán *et al.,*** 2018) and the onset of the change of the real part of the dielectric permittivity for all compounds with R=Eu, Sm, and Dy. This transition has to do with the change between a paraelectric state (T>113 K) and a ferroelectric state (T<113 K), which has its origin in a structural transition between the centrosymmetric space group Pnma and another polar group (non-centrosymmetric), the I4/mcm, which has the low global instability index characteristic of some of the perovskite materials reach ordering of the dipole moments at low temperatures (**Mishra & Pandey,** 2009).

In a complete study of this material under pressures up to 18 GPa, a shift of the transition towards higher temperature regimes was observed (**Gil-Rebaza *et al*.,** 2021). This Curie temperature shift is due to the increase in pressure decreasing the overlap between

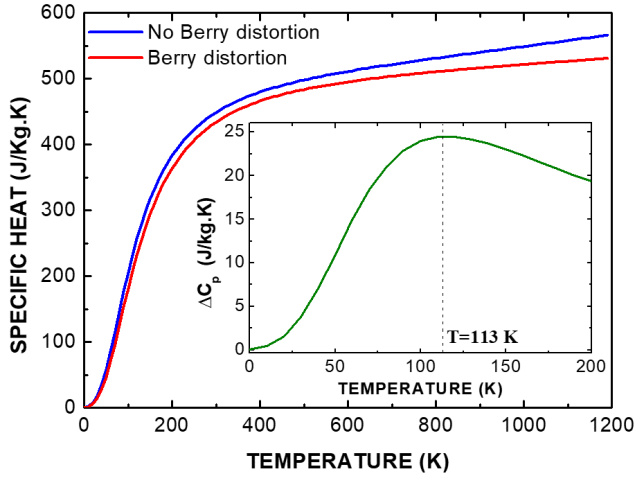

Figure 7. Phase transition observed in the specific heat related to ferroelectric ordering at T=113 K in $Bi_{0.5}Eu_{0.5}FeO_3$. The inset clearly shows the change in the specific heat difference with and without the Berry phase.

the Fe-3d(e_g) and O-2p orbitals in the FeO_6 octahedra of the material, as expected for any insulating perovskite and in oxide material molecules (**Korney *et al.,*** 2005; **Korney & Bellaiche,** 2007).

This type of response is expected in multiferroic materials in which the effect of pressure can induce changes in the ferroelectric response (**Ding & Shong**, 2020), as well as in the occurrence of the magnetoelectric coupling (**Gilioli & Ehm**, 2014) taking place at T=113 K induced by the Dzyaloshinskii-Moriya-type interactions (**Sergienko *et al.,*** 2006; **Fodouop *et al.***, 2019) associated with the partial tilting of magnetic moments in perovskite octahedra (**Dong *et al.,*** 2019). The interaction mechanisms are favored by hybridizations between the 3d-Fe and 2p-O orbitals in the octahedra, which result in the ferromagnetic character in the density of states calculation in **figures 6a** and **6c**.

Conclusions

Rare earth perovskite-like ferrocobaltite $Bi_{0.5}R_{0.5}FeO_3$ (R=Eu, Sm, and Dy) were successfully synthesized using the solid-state reaction method. The structural analysis showed that these materials crystallize in orthorhombic structures belonging to the Pnma space group (number 62) with strong octahedral distortions and cationic disorder of Bi^{3+} and R^{3+} along the crystallographic axes. The weak ferromagnetic nature of these perovskite materials was established from the hysteretic curves of magnetization as a function of applied field strengths at 50, 200, and 300 K. Dielectric measurements have shown a Maxwell-Wagner-type relaxation process, probably aroused from the depletion layers due to the electrode-sample interfaces and irregular intergranular boundaries. The pyroelectric current and magnetic response characterizations suggested that the $Bi_{0.5}R_{0.5}FeO_3$ perovskites behave as biferroic materials below T=113 K. The analysis of the experimental diffuse reflectance data showed that these materials behave as semiconductors at room temperature with their insulating character expected at temperatures close to 113 K, where the material must also undergo a structural transition to a non-centrosymmetric system that promotes a transition from the ferromagnetic-paraelectric state at high temperatures to the ferromagnetic-ferroelectric state at low temperatures.

We complemented the analysis of the physical properties of the material with a theoretical analysis by means of calculations considering the structural space group Pnma emerging from the experimental results. The density-of-state calculations suggest the appearance of a semiconductor-like behavior with a band gap of 1.76 eV explained by the majority contribution of the 2p-O orbitals in the valence band and the hybridization with the 4f-R and 6p-Bi orbitals. For their part, the Fe cation displacements applied through the Berry-phase study should promote a structural modification between the centrosymmetric space group and a polar (non-centrosymmetric) cell type to promote the spontaneous formation of dipole moments. The octahedral distortions introduced by the Berry phase give rise to Dzyaloshinskii-Moriya interactions that allow the coexistence of the spontaneous ferroelectric electric polarization and the weak ferromagnetic response due to canting effects on the ordered spins. Thus, a marked increase in the value of the forbidden band is obtained when the density of states is determined considering the Berry phase. The macroscopic polarization of the material was calculated through the Berry phase and the result was consistent with the experimental analysis as the behavior had a ferroelectric characteristic. The difference in the specific heat between the states with and without the Berry phase suggests the occurrence of a transition at T = 113 K in agreement with the experimental observations through thermostimulated and pyroelectric currents.

While the biferroic nature of the material $Bi_{0.5}R_{0.5}FeO_3$ is associated with low temperatures, its technological relevance at room temperature is related to the coexistence of the ferromagnetic response and semiconductivity in a single crystallographic phase, which could take place for a whole family of rare earths at the R site, suggesting a new line of research in the design of devices based on spintronic technology of ceramic materials applied for the simultaneous control of the transport of electric charge carriers and spin

currents since the asymmetry in the band structure in the vicinity of the Fermi level for the spin-up and spin-down orientations gives rise to a new magnetic spin transport channel. These characteristics open the possibility of using lanthanide ferrocobaltite-type materials in technological devices based on polarized spin currents, such as spin valves and novel spin transistors, in which, besides the control of the transport of electronic carriers, the presence of low external magnetic fields favors the control of the parameters related to the transport of magnetic moments. Additionally, the biferroic character at low temperatures (113 K) creates a reflective space around the prospect of tuning the magnetoelectric transition temperature through compositional modifications or by applying hydrostatic pressures thereby increasing the number of degrees of freedom and versatility of spintronic properties in the material.

It is worth noting that the coexistence of these two physical properties (the ferromagnetic character and the semiconductor response) at room temperature opens up application possibilities for this family of materials in devices such as ferromagnetic transistors that adopt multifunctional characteristics as the writing, erasing, and reading procedures of magnetic information can be performed while simultaneously processing activities, with the particularity that the polarized spin currents guarantee a higher response speed in these spintronic processes.

Acknowledgements

This work received partial support from the DIEB-ORI at the National University of Colombia (Hermes Code 52594) and FONCIENCIAS at *Universidad del Magdalena*.

Author contributions

JRR proposed and directed the project, coordinated the work team, interpreted and correlated the experimental and theoretical results, analyzed the interaction mechanisms, and wrote the paper. JACF synthesized the samples and performed the structural, morphological, and electrical characterizations. CEDT performed the theoretical calculations. DALT coordinated the structural and morphological analyses. CAPV performed the magnetic characterization.

Conflicts of interest

The authors declare that there is no conflict of interests of any kind regarding the publication of the results of our research work.

References

Acharya, S., Mondal, J., Ghosh, S., Roy, S.K., Chakrabarti, P.K. (2010). Multiferroic Behavior of Lanthanum Orthoferrite ($LaFeO_3$). *Materials Letters*, *64*, 415-418.

Alarcón-Suesca, C.E., Deluque-Toro, C.E., Gil-Rebaza, A.V., Landínez-Téllez, D.A., Roa-Rojas, J. (2019). Ab-initio studies of electronic, structural and thermophysical properties of the Sr_2TiMoO_6 double perovskite. *Journal of Alloys and Compounds*, *771*, 1080-1089.

Benedek, N.A. (2014). Origin of Ferroelectricity in a Family of Polar Oxides: The Dion—Jacobson Phases. *Journal Inorganic* Chemistry, *53*, 3769-3777.

Blöchl, P.E. (1994). Projector augmented-wave method. *Physical Review Journals, 50*, 17953-17979.

Brown, I.D. (2009). Recent Developments in the Methods and Applications of the Bond Valence Model. *Journal Chemical Reviews*, *109* (12), 6858-6919

Cuervo-Farfán, J.A., Aljure-García, D.M., Cardona, R., Arbey-Rodríguez, J., Landínez-Téllez, D.A., Roa-Rojas, J. (2017). Structure, Ferromagnetic, Dielectric and Electronic Features of the $LaBiFe_cO_6$ Material. *Journal of Low Temperature Physics*, *186*, 295-315.

Cuervo-Farfán, J.A., Castellanos-Acuña, H.E., Landínez-Téllez, D.A., Parra-Vargas, C.A., Roa-Rojas, J. (2016). Structural, magnetic, and electrical features of the $Nd_2SrMn_2TiO_9$ perovskite-like compound, *Physica Status Solidi (B)*, *253*, 1127-1132.

Cuervo-Farfán, J.A., Deluque-Toro, C.E., Parra-Vargas, C.A., Landínez-Téllez, D.A., Roa-Rojas, J. (2020). Experimental and theoretical determination of physical properties in the $Sm_2Bi_2Fe_4O_{12}$ ferromagnetic semiconductor. *Journal of Materials Chemistry*, *C8*, 4925-14939.

Cuervo-Farfán, J.A., Parra-Vargas, C.A., Viana D.S.F., Milton, F.P., García, D., Landínez-Téllez, D.A., Roa-Rojas, J. (2018). Structural, Magnetic, Dielectric and Optical Properties of the $Eu_2Bi_2Fe_4O_{12}$ Bismuth-Based Low-Temperature Biferroic, *Journal of Materials Science: Materials in Electronics*, *29*, 20942-20951.

Cuervo-Farfán, J.A., Benav.des-Lara, J.P., Parra-Vargas, C.A. Landínez-Téllez, D.A., Roa-Rojas, J. (2021). Structural Characteristics and Electric and Magnetic Features of the $Nd_{2.68}Sr_{1.32}Mn_{1.2}Ti_{1.32}Fe_{1.48}O_{12}$ Ferromagnetic Semiconductor. *Journal of Low Temperature Physics*, *202*, 128-144.

Dann, S.E., Currie, D.B., Weller, M.T., Thomas, M.F., Al-Rawwas, A.D. (1994). The Effect of Oxygen Stoichiometry on Phase Relations and Structure in the System $La_{1-x}Sr_xFeO_{3-\delta}$ ($0 \leq x \leq 1$, $0 \leq \delta \leq 0.5$). *Journal of Solid State Chemistry*, *109*, 134-144.

Dash, U., Sahoo, S., Chaudhuri, P., Parashar, S.K.S., Parashar, K. (2014). Electrical properties of bulk and nano Li_2TiO_3 ceramics: A comparative study. *Journal of Advanced Ceramics*, *3*, 89-97.

Deluque-Toro, C.E., Mosquera-Polo, A.S., Gil-Rebaza, A.V, Landínez-Téllez, D.A., Roa-Rojas, J. (2018a). Ab Initio Study of the Electronic Structure, Elastic Properties, Magnetic Feature and Thermodynamic Properties of the Ba_2NiMoO_6 Material. *Journal of Low Temperature Physics*, *192*, 265-285.

Deluque-Toro, C.E., Mosquera-Polo, A.S., Villa-Hernández, J.I., Landínez-Téllez, D.A., Roa-Rojas, J. (2018b). Thermodynamic properties, electronic and crystallographic structure, and magnetic response of the Sr_2HoNbO_6 material. *Revista de la Academia Colombiana de Ciencias Exactas, Físicas y Naturales*, *42*,180-187.

Deluque-Toro, C.E., Landínez-Téllez, D.A., Roa-Rojas, J. (2018). Ab-initio analysis of magnetic, structural, electronic and thermodynamic properties of the Ba_2TiMnO_6 manganite. *DYNA, 85*, 27-36.

Ding, J.L & Zhong, Y. (2020). A theoretical strategy for pressure-driven ferroelectric transition associated with critical behavior and magnetoelectric coupling in organic multiferroics. *Physical Chemistry Chemical Physics*, *22*, 19120-19130.

Dong, S., Xiang, H., Dagotto, E. (2019). Magnetoelectricity in multiferroics: a theoretical perspective. *National Science Review*, *6*, 629-641.

Estrada-Contreras, V.R., Alarcón-Suesca, C.E., Deluque-Toro, C.E., Landínez-Téllez, D.A., Roa-Rojas, J. (2021). Crystalline, ferromagnetic-semiconductor and electronic features of the terbium-based cobalt-ferrite Tb_2FeCoO_6. *Ceramics International*, *47*, 14408-14417.

Fodouop, F.K., Fouolceng, G.C., Tchoffo, M., Fai, L.C., Randrianantoandro N. (2019). Thermodynamics of metamagnetoelectric effect in multiferroics. *Journal of Magnetism and Magnetic Materials*, *474*, 456-461.

Garrido, L.C., Deluque-Toro, C.E., Díaz, I., Landínez-Téllez, D.A., Roa-Rojas, J. (2021). First-principles calculations to investigate elastic, electronic and thermophysical properties of the $Dy_2Bi_2Fe_4O_{12}$ ferromagnetic semiconductor. *Semiconductor Science and Technology*, *36*, 095015.

Gil-Rebaza, A.V., Deluque-Toro, C.E., Medina-Chanduví, H.H., Landínez-Téllez, D.A., Roa-Rojas, J. (2021). Thermodynamic evidence of the ferroelectric Berry phase in europium-based ferrobismuthite $Eu_2Bi_2Fe_4O_{12}$. *Journal of Alloys and Compounds*, *884*, 161114.

Gilioli, E. & Ehm, L. (2014). High pressure and multiferroics materials: a happy marriage. *IUCrJ, 1*, 590-603.

Glazer, A.M. (1975). Simple ways of determining perovskite structures. Acta Crystallographica, *31*, 756-762.

Goldschmidt, V.M. (1926). Die Gesetze der Krystallochemie. *Naturwissenschaften*, *14* (21), 477-485

Guss, P., Foster, M.E., Wong, B.M., Doty, F.P., Shah, K., Squillante, M.R., Shirwadkar, U., Hawrami, R., Tower, J., Yuan, D. (2014). Results for aliovalent doping of $CeBr_3$ with Ca^{2+}. *Journal of Applied Physics*, *15*, 034908.

Hazen, R.M. (1988). Perovskites. *Scientific American*, *258*, 74-81.

Heyd, J., Scuseria, G.E., Ernzerhof, M. (2003). Hybrid functionals based on a screened Coulomb potential. *Journal of Chemical Physics*, *118*, 8207-8215.

Jaramillo-Palacio, J.A., Barrera-Bello, E.W., Munévar-Cagigas, J.A., Arnache, O., Landínez-Téllez, D.A., Roa-Rojas, J. (2017). Structure and Physical Properties of the $LaBiFe_2O_6$ Perovskite Produced by the Modified Pechini Method. *Journal of Materials Research*, *20*, 1309-1316.

Jaramillo-Palacio, J.A., Muñoz-Pulido, K.A., Arbey-Rodríguez, J., Landínez-Téllez, D.A., Roa-Rojas, J. (2021). Electric, magnetic and microstructural features of the La_2CoFeO_6 lanthanide ferrocobaltite obtained by the modified Pechini route. *Journal of Advanced Dielectrics*, *11*, 2140003.

King, G. & Woodward, P.M. (2010). Cation ordering in perovskites. *Journal of Materials Chemistry*, *20*, 5785-5796.

Koehler, W.C. & Wollan, E.O. (1957). Neutron-diffraction study of the magnetic properties of perovskite-like compounds $LaBO_3$. *Journal of Physics and Chemistry of Solids*, *2*, 100-106.

Kresse, G. & Joubert, J. (1999). From ultrasoft pseudopotentials to the projector augmented-wave method. *Physical Review B*, *59*, 1758-1775.

Landínez-Téllez, D.A., Buitrago-Martínez, D., Barrera, E.W., Roa-Rojas, J. (2014). Crystalline structure, magnetic response and electronic properties of RE_2MgTiO_6 (RE= Dy, Gd) double perovskites. *Journal of Molecular Structure*, *1067*, 205-209.

Liechtenstein, A.I., Anisimov,V.I., Zaanen, J. (1995). Density-functional theory and strong interactions: Orbital ordering in Mott-Hubbard insulators. *Physical Review* B, *52*, R5467-R5470.

Llamosa, D.P., Landínez-Téllez, D.A., Roa-Rojas, J. (2009). Magnetic and structural behavior of Sr_2ZrMnO_6 double perovskite. *Journal of Physics B*, *404*, 2726-2729.

Lu, J., Günther, A., Schrettle, F., Mayr, F., Krohns, S., Lunkenheimer, P., Pimenov, A., Travkin, V.D., Mukhin, A.A., Loidl, A. (2010). On the Room Temperature Multiferroic BiFeO3: Magnetic, Dielectric and Thermal Properties. *European Physical Journal B*, *75*, 451-460.

Lufaso, M.W. & Woodward, P.M. (2001). Prediction of the Crystal Structures of Perovskites Using the Software Program SPuDS. *Acta Crystallographica, B57*, 725-738.

Lunkenheimer, P., Bobnar, V., Pronin, A.V., Ritus, A.I., Volkov, A.A., Loidl, A. (2002). Origin of apparent colossal dielectric constants. *Journal of Physics B*. *66,* 521051.

Methfessel, M. & Paxton, A.T. (1986). High-precision sampling for Brillouin-zone integration in metals. *Journal of Physics B*, *40*, 3616-3621.

Mishra, S.K. & Pandey, D. (2009). Low temperature x-ray diffraction study of the phase transitions in $Sr_{1-x}Ca_xTiO_3$ (x=0.02,0.04): Evidence for ferrielectric ordering. *Applied Physics Letters*, *95*, 232910.

Monkhorst, H.J. & Pack, J.D. (1976). Special points for Brillouin-zone integrations. *Journal of Physics B*, *13*, 5188-5192.

Murnaghan, F.D. (1944). The Compressibility of Media under Extreme Pressures. *Proceedings of the National Academy of Sciences*, *30*, 244-247.

Myrick, M.L., Simcock, M.N., Baranowski, M., Brooke, H., Morgan, S.L., McCutcheon, J.N. (2011), The Kubelka-Munk Diffuse Reflectance Formula Revisited. *Applied Spectroscopy Reviews*, *46*, 140-165.

Nieto-Camacho, J.A., Cardona-Vásquez, J.A., Sarmiento-Santos, A., Landínez-Téllez, D.A., Roa-Rojas, J. (2020). Study of the microstructure and the optical, electrical, and magnetic feature of the $Dy_2Bi_2Fe_4O_{12}$ ferromagnetic semiconductor, *Journal of Materials Research and Technology*, *9*, 10686-10697.

Pandey, R.K., Stapleton, W.A., Sutanto, I. (2015). Nature and Characteristics of a Voltage-Biased Varistor and its Embedded Transistor. *IEEE Journal of the Electron Devices Society*, *3*, 276-283

Perdew, J.P., Burke, K., Ernzerhof, M. (1996). Generalized Gradient Approximation Made Simple. *Physical Review Letters*, *77*, 3865-3868.

Phokha, S., Pinitsoontorn, S., Maensiri, S., Rujirawat, S. (2014). Structure, optical and magnetic properties of $LaFeO_3$ nanoparticles prepared by polymerized complex method. *Journal of Sol-Gel Science and Technology*, *71*, 333-341.

Resta, R. (1994). Macroscopic polarization in crystalline dielectrics: the geometric phase approach. *Reviews of Modern Physics*, *66,* 899-915.

Resta, R. (1997). Polarization as a Berry Phase, *Europhys. News, 28*, 18-20.

Sergienko, I.A. & Dagotto, E. (2006). Role of the Dzyaloshinskii-Moriya interaction in multiferroic perovskites *Journal of Physics B*, *73*, 094434.

Sorescu, M., Xu, T., Hannan, A. (2011). Initial Stage Growth Mechanism of $LaFeO_3$ Perovskite through Magnetomechanical Ball-Milling of Lanthanum and Iron Oxides. *American Journal of Materials Science*, *1*, 57-66.

Spaldin, N.A. (2020). Multiferroics beyond electric-field control of magnetism. *Proceedings of the Royal Society A*, *476*, 20190542.

Triana, C.A., Landínez-Téllez, D.A., Roa-Rojas, J. (2012). Synthesis process and structural characterization of the Sr_2EuRuO_6 complex perovskite. *Journal of Alloys and Compounds*, *516*, 179-185.

Vojta, A., Wen, Q., Clarke, D.R. (1996). Influence of microstructural disorder on the current transport behavior of varistor ceramics. *Computational Materials Science*, *6*, 51-62.

Wu, J., Mao, S., Ye, Z-G., Xie, Z., Zheng, L. (2010). Room-temperature ferromagnetic/ferroelectric $BiFeO_3$ synthesized by a self-catalyzed fast reaction process. *Journal of Materials Chemistry A*, *20*, 6512-6516.

Xu, J.M., Wang, G.M., Wang, H.X., Ding, D.F., He, Y. (2009). Synthesis and weak ferromagnetism of Dy-doped $BiFeO_3$ powders. *Materials Letters, 63*, 855–857.

Yamada, I., Takamatsu, A., Ikeno, H. (2018). Complementary evaluation of structure stability of perovskite oxides using bond-valence and density-functional-theory calculations. *Science and Technology of Advanced Materials*, *19* (1), 101-107.